Meteoritics & Planetary Science 1–18 (2016)
doi: 10.1111/maps.12711

Report

Distinction between amorphous and healed planar deformation features in shocked quartz using composite color scanning electron microscope cathodoluminescence (SEM-CL) imaging

Maartje F. HAMERS[1], Gill M. PENNOCK[1,*], Marco HERWEGH[2], and Martyn R. DRURY[1]

[1]Department of Earth Sciences, Faculty of Geosciences, Utrecht University, Budapestlaan 4, 3584 CD, Utrecht, the Netherlands
[2]Institute of Geological Sciences, University of Bern, Baltzerstrasse 1 + 3, CH-3012 Bern, Switzerland
[*]Corresponding author. E-mail: g.m.pennock@uu.nl

(Received 10 November 2015; revision accepted 24 June 2016)

Abstract–Planar deformation features (PDFs) in quartz are one of the most reliable and most widely used forms of evidence for hypervelocity impact. PDFs can be identified in scanning electron microscope cathodoluminescence (SEM-CL) images, but not all PDFs show the same CL behavior: there are nonluminescent and red luminescent PDFs. This study aims to explain the origin of the different CL emissions in PDFs. Focused ion beam (FIB) thin foils were prepared of specific sample locations selected in composite color SEM-CL images and were analyzed in a transmission electron microscope (TEM). The FIB preparation technique allowed a direct, often one-to-one correlation between the CL images and the defect structure observed in TEM. This correlation shows that composite color SEM-CL imaging allows distinction between amorphous PDFs on one hand and healed PDFs and basal Brazil twins on the other: nonluminescent PDFs are amorphous, while healed PDFs and basal Brazil twins are red luminescent, with a dominant emission peak at 650 nm. We suggest that the red luminescence is the result of preferential beam damage along dislocations, fluid inclusions, and twin boundaries. Furthermore, a high-pressure phase (possibly stishovite) in PDFs can be detected in color SEM-CL images by its blue luminescence.

INTRODUCTION

The presence of planar deformation features (PDFs) in quartz is one of the most reliable forms of evidence for the impact origin of suspected geological structures or stratigraphic layers. PDFs are planar microstructures that form in quartz and other minerals (e.g., feldspar) as a result of a shock wave passing through the rocks (e.g., papers in French and Short 1968; von Engelhardt and Bertsch 1969; Stöffler and Langenhorst 1994; Grieve et al. 1996) and can be observed in standard thin sections in a standard petrographic microscope. Because PDFs are so widely used as impact evidence, their correct identification is crucial. However, using light microscopy PDFs can look very similar to nonimpact-related (sub)planar microstructures, such as healed fractures or tectonic deformation lamellae (e.g., Christie and Raleigh 1959; Christie and Ardell 1974; Drury 1993; Vernooij and Langenhorst 2005). Therefore, transmission electron microscopy (TEM) observations on the submicron scale structure of the lamellae are often necessary to distinguish between shock and nonshock-related structures and to confirm the shock origin of planar microstructures in quartz (e.g., Stöffler and Langenhorst 1994; Grieve et al. 1996; French and Koeberl 2010). However, TEM facilities are expensive and not readily available to many researchers. In addition, TEM studies involve difficult and time-consuming sample preparation and often require extensive training.

Recently, Boggs et al. (2001) and Hamers and Drury (2011) showed that in addition to TEM,

cathodoluminescence (CL) imaging in the scanning electron microscope (SEM) is a reliable method to distinguish between shock-related and tectonically formed planar microstructures in quartz. Although Boggs et al. (2001) concluded that PDFs show no CL emission at all, Hamers and Drury (2011) demonstrated that composite color SEM-CL imaging shows two main types of CL behavior in PDFs: red luminescence and nonluminescence. Also Gucsik et al. (2015) observed nonluminescent PDFs in shocked quartz grains from the Ries crater. The reason for the different CL emissions, however, remained unclear.

In this paper, we aim to clarify the differences in CL emissions from PDFs in quartz as observed in Hamers and Drury (2011). In order to identify the relationship between CL emission and the microstructure of PDFs in quartz, we performed TEM analysis on both red and nonluminescent PDFs. To control the exact location of the TEM samples and to enable a direct, often one-to-one comparison of PDFs in SEM-CL and TEM images, the TEM samples were prepared using a focused ion beam (FIB) (Wirth 2004, 2009). In addition, CL spectroscopic measurements of the emission of red luminescent PDFs were done to provide an indication of the defects that are responsible for the red CL emission. Furthermore, we analyze the effect on CL emission of prolonged exposure of the quartz grains to the electron beam and we show results suggesting that a high-pressure phase, possibly stishovite, can be detected in SEM-CL images.

Directly comparing SEM-CL images with results from TEM techniques that are universally accepted as effective tools for PDF identification and analysis (see reviews by Stöffler and Langenhorst 1994; Grieve et al. 1996; French and Koeberl 2010), with the addition of CL spectroscopy, will help to determine the source of the CL emission and thereby validate the SEM-CL method to identify and characterize PDFs in quartz.

Planar Deformation Features in Quartz

PDFs consist of thin (<1 μm), parallel, closely spaced (typically <2 μm apart) lamellae. Usually multiple (normally ~2–4) sets of PDFs develop in the same grain (von Engelhardt and Bertsch 1969; Stöffler and Langenhorst 1994; Grieve et al. 1996; French and Koeberl 2010). Although PDFs are generally described as strictly straight and planar, some bending or slight curvature has been reported (von Engelhardt and Bertsch 1969; Stöffler and Langenhorst 1994; Trepmann and Spray 2005). PDFs can be penetrative through a whole grain or occur in parts of a grain, but do not cross grain boundaries, cracks, faults, or fractures that were present before PDF formation.

PDFs have a crystallographically determined orientation parallel to low-index rational planes (most frequently observed are the basal c(0001) and $\omega\{10\bar{1}2\}$ and $\pi\{10\bar{1}3\}$ type planes) (Stöffler and Langenhorst 1994; Ferrière et al. 2009). Unaltered or "fresh" PDFs are thin lamellae of amorphous silica, formed under high pressure during shock compression. Basal PDFs, parallel to c(0001), are not amorphous, but consist of mechanical Brazil twins. In shock experiments on quartz, Langenhorst (1994) observed that at relatively low peak shock pressures (<25 GPa), rhombohedral PDFs are extremely narrow (~30 nm), but around 25 GPa, thickness increases to >200 nm and PDFs can become slightly curved and show thickness variations along their length.

During postshock high temperature or metamorphic events, amorphous PDFs can easily recrystallize. Healed PDFs are recognized in TEM as planes with a very high dislocation density (e.g., Goltrant et al. 1991, 1992; Trepmann and Spray 2006). In light microscopy, they are observed as traces of fluid inclusions along the original PDF plane (known as "decorated PDFs"), of which the crystallographic orientation can still be measured in the universal stage (e.g., Ferrière et al. 2009). Because amorphous PDFs only occur in relatively fresh, unaltered impact material, it is useful to be able to easily detect the presence of amorphous PDFs in shocked quartz. Furthermore, the presence of amorphous material can help identify microlamellae in quartz as PDFs, as microstructures that are often misinterpreted as PDFs (e.g., tectonic deformation lamellae) do not contain amorphous material. At present, the most widely applied method to detect amorphous PDFs is TEM analysis (e.g., Goltrant et al. 1991, 1992; Langenhorst 1994, 1996; Trepmann and Spray 2006).

Cathodoluminescence

In a material that is scanned by the electron beam in the SEM, electrons in the sample are excited to a higher band level by the incoming energy of the beam. When the excited electrons fall back to their original energy state, photons are emitted. This phenomenon is known as cathodoluminescence. The wavelength spectrum and intensity of photon emission depend on the material and crystallographic defects and on the presence of trace elements or fluids in the sample. In quartz, CL emission depends on many factors such as the degree of ordering in the crystal lattice; vacant lattice sites; impurities such as Fe^{3+}, Al^{3+}, and H^{+}; water content; or damage resulting from radiation, strain, or shock (Marshall 1988; Ramseyer and Mullis 1990; Perny et al. 1992). Common emission bands in

crystalline α-quartz are around 340 nm (Al and Li impurities), 420 nm (intrinsic emission), and 620–650 nm (nonbridging oxygen hole center, NBOHC, $O_3{\equiv}Si\text{-}O\cdot$, i.e., a dangling oxygen bond, that is bonded to a silicon atom attached to three other oxygen atoms) (Stevens Kalceff and Phillips 1995; Stevens Kalceff et al. 2000; Götze et al. 2001; Stevens Kalceff 2009), but many more emission bands are described in the literature. The relative intensities of the dominant emission bands in the visible light range (380–700 nm, blue to red) determine the CL color that is perceived by the eye (Götze et al. 2001).

Shocked quartz is generally blue luminescent, with an additional emission band at 630–650 nm (Ramseyer et al. 1992; Ramseyer and Mullis 2000; Trepmann et al. 2005; Götte 2009). Boggs et al. (2001) first demonstrated the potential of SEM-CL to image PDFs in quartz and concluded that PDFs are nonluminescent in grayscale SEM-CL images. Hamers and Drury (2011), however, using a CL detector with a broader detection range and color filters, showed that in composite color SEM-CL images, PDFs can have different CL characteristics. Some are indeed nonluminescent, but many are red luminescent and also "intermediate" cases were observed, with both red and nonluminescent (parts of) PDFs in the same grain.

MATERIALS AND METHODS

The quartz grains described in this study are mostly naturally shocked grains from different impact structures (El'gygytgyn, Ries, Popigai, Rochechouart, and Vredefort). The same shocked quartz samples were studied here as were described by Hamers and Drury (2011) and in addition SEM-CL images were recorded of a granitic sample from the Vredefort structure in South Africa, quartz grains in a reworked suevite sample from the El'gygytgyn crater in Russia (ICDP drill core, Raschke et al. 2013), an experimentally shocked (23.5 GPa) Hospital Hill quartzite, and an experimentally shocked (24 GPa) single crystal. The experimentally shocked samples were previously studied and described by Reimold and Hörz (1986a, 1986b) (Hospital Hill quartzite) and Fritz et al. (2011) (single crystal). In total, 12 TEM foils were studied. Table 1 lists the new samples and the TEM foils, with their locations, main characteristics, and the observed microstructures.

Composite color SEM-CL images were recorded at the Electron Microscopy Utrecht lab (EMU), the Netherlands, using a FEI Nova Nanolab 600 dual beam SEM with focused ion beam (FIB) and Gatan PanaCL detector with a detection range of 185–850 nm. Acceleration voltages of 5–10 kV were used, with beam currents of 1.6–6.3 nA, at room temperature. The procedures are described in detail in Hamers and Drury (2011). The CL signal is emitted from the whole interaction volume. Monte Carlo simulations using Casino v2.42 software (Drouin et al. 2007) indicate that an electron beam with an energy of 5–10 kV penetrates into the sample to a maximum depth of ~0.1–3 μm. This gives an indication of the imaging resolution under the conditions used in this study.

TEM foils with a thickness of ~100–200 nm were prepared in the same FIB-SEM instrument, using a standard in situ lift-out procedure (Wirth 2004, 2009), with an acceleration voltage of 30 kV and beam currents ranging from 20 nA down to 0.3–0.5 nA for the final polishing steps. The FIB-SEM preparation of the TEM foils allows a direct, often one-to-one correspondence of PDFs in TEM and SEM-CL images.

TEM analysis was carried out on an FEI Tecnai 20 FEG instrument, also at EMU, operated at 200 kV, with double tilt holder. Bright-field (BF) TEM imaging was used to show the microstructure in the samples. Diffuse dark-field (DDF) TEM images showed the presence of amorphous material. In DDF images, amorphous areas are bright, while crystalline material is dark. In addition, tilting the sample in BF mode showed whether there was any diffraction contrast associated with crystallinity.

CL spectroscopic measurements were performed on a polished, carbon-coated thin section of sample RI-37 (Ries, see Table 1) with red luminescent PDFs, on a Zeiss EVO 50 instrument with Gatan MonoCL 3 system, at the Institute of Geological Sciences in Bern, Switzerland. Spectra of the red luminescent PDFs and the host quartz were recorded with a PIXIS 100 CCD camera (Princeton Instruments). The CCD has nearly constant detector efficiency for the visible light wavelength range. Grating of the spectroscopic system was set to 300 lines/mm with a slit size of 2 mm. Spectra were recorded in a 600 nm range and with a central wavelength of 500 nm, resulting in simultaneous measurement of the 200–800 nm spectra. Acceleration voltages of 5–8 kV were used, with beam currents of 1.4–3 nA at room temperature. PDFs are too narrow to measure directly by spot measurements, because the interaction volume of the electron beam with the quartz is too large to only sample the PDF. Inevitably some of the surrounding quartz is sampled by the beam. To overcome this problem, spectra were measured from areas with a high density of PDFs and areas without PDFs in the same grain. The ratio of the intensity of the main peaks between PDFs and host grain was then determined. Measurements were done in areas of the sample that had not been scanned by the electron beam before, with a measurement time of 30 seconds. Because only peak ratios were considered and not absolute

Table 1. Sample locations and properties of studied TEM foils and new samples studied by SEM-CL.

Sample	Location	lat/lon (WGS84)	Rock type	TEM section	CL emission of PDFs	PDF microstructure in TEM	Grain microstructure in TEM
RI-37	Ries (Germany), Auhmühle	48°58′16.84″N/10°37′43.95″E	Granite fragment (loose block, probably from suevite)	RI-37_01	Red	Dislocations	Single crystal, some dislocations
RI-37-1	Ries (Germany), Auhmühle	48°58′16.84″N/10°37′43.95″E	Granite fragment (loose block, probably from suevite)	RI-37-1_71	Red	Dislocations	Single crystal, some dislocations
OTT-2	Ries (Germany), Otting	48°52′32.07″N/10°47′42.37″E	Suevite	OTT-2_17	No/red	Mixed	Single crystal
				OTT-2_22	No	Amorphous	(Micro?)crystalline
MRO-5-1	Rochechouart (France), Montoume	45°46′31.94″N/0°46′30.01″E	Impact melt rock	MRO-5-1_02	Red	Dislocations	Single crystal, some dislocations
				MRO-5-1_05	Red	Dislocations	Mosaic
				MRO-5-1_05A	Red	Dislocations	Mosaic
55	Vredefort (South Africa)	W of Parys, exact location unknown	Granite gneiss	55_03_1	Red	Brazil twins	Single crystal, some dislocations
				55_03_2	Red	Brazil twins	Single crystal, some dislocations
				55_07	Red	Brazil twins	Single crystal, some dislocations
				55_07A	Red	Brazil twins	Single crystal, some dislocations
1270	Experimental		Quartzite, experimentally shocked, 23.5 GPa (see also Reimold and Hörz 1986a, 1986b)	1270_01	No	Amorphous	(Micro?)crystalline
24	Experimental		Quartz single crystal (see Fritz et al. 2011)	—	No/blue	—	—
320.27	El'gygytgyn	67°30′N/17°05′E	Suevite (probably reworked, see Raschke et al. 2013)	—	No/red	—	—

values, no correction for detector response was carried out.

RESULTS

Nonluminescent PDFs

Figure 1 shows CL (a and d) and TEM (b, c, e, and f) images of two grains with nonluminescent PDFs, in a suevite from the Ries crater in Germany (a, b, c) and in a quartzite experimentally shocked to 23.5 GPa (d, e, f). In bright-field TEM images (Figs. 1b and 1e), the PDFs are always a uniform gray, irrespective of tilt angle. In corresponding diffuse dark-field images of the same area (Figs. 1c and 1f), PDFs are brighter than the surrounding material. Both bright-field and diffuse dark-field characteristics of nonluminescent PDFs therefore indicate that they are amorphous. The corresponding diffraction patterns (insets in Figs. 1b and 1e) show diffuse scattering intensity (similar to, e.g., diffraction patterns shown by Cordier and Gratz [1995] and Langenhorst [1996]) and are consistent with the presence of amorphous material in the sample. The diffraction patterns from nonluminescent PDFs show considerably more diffuse intensity than those from red luminescent PDFs (e.g., Fig. 2b). In addition to diffuse intensity, a broad, diffuse halo is present in the diffraction pattern as shown in Fig. 1e, just inside the $10\bar{1}0$ diffraction maxima (4.26 Å), which is consistent with d-spacings for fused silica reported in the literature (4.12 Å, e.g., Lana and Seddon 1998). Diffuse halos can be hard to distinguish from inelastic scattering in a diffraction pattern, which can occur in thick foils. However, the foils used in this study have a thickness of 100–200 nm, which is not particularly thick for quartz when using 200 kV electrons. Furthermore, there is no evidence of Kikuchi bands in the diffraction patterns, which are normally observed in thick sections.

The quartz in between the PDFs is diffracting and therefore crystalline. Slight streaking of the (outer) diffraction spots (insets in Figs. 1b and 1e) points to a small misorientation between the crystalline domains. Dislocations and other defects were not observed in the crystalline quartz.

Red Luminescent PDFs

Figures 2–4 show that red luminescent PDFs can be either healed structures (Figs. 2 and 3) or basal Brazil twins (Fig. 4).

Figures 2a–c (Rochechouart) show that the red luminescent PDFs in this sample are planes of high dislocation density or arrays of dislocations, similar to microstructures observed in healed PDFs in earlier studies (e.g., Goltrant et al. 1991; Trepmann and Spray 2006). In grains like the one shown in Figs. 2a–c, with few sets and a relatively low density of PDFs, the crystalline host quartz is a single crystal and not microcrystalline; there are no misorientations in the grain (no streaking of diffraction spots occurs, see inset in Fig. 2b). Aside from in the PDF planes, only a few dislocations are present in the grain. In Figs. 2b and 2c, a Dauphiné twin boundary can be traced from the upper right corner along a PDF, then crossing to another PDF and following this PDF's orientation. In rare cases, such as the grain from the Ries crater in Fig. 2d, SEM-CL images show that red luminescent PDFs consist of small sublamellae (black arrow in Fig. 2d) in a configuration similar to the dislocation arrays observed in TEM.

In a grain from the Vredefort Dome, red luminescent PDFs (Fig. 3a) consist of basal Brazil twins (shown edge-on in bright-field TEM in Fig. 3b and tilted in Fig. 3c). Some dislocations are present in this grain and parts of the Brazil twin boundaries are decorated with dislocations. However, there are also segments of the twin boundaries that are free of dislocations. It therefore appears that the red CL emission comes from the twin boundaries themselves and not (only) from dislocations, as opposed to the red luminescent PDFs shown in Fig. 2.

Red and Nonluminescent PDFs

Besides the red and nonluminescent endmembers of CL behavior that PDFs exhibit in SEM-CL, an intermediate type occurs: grains with both red and nonluminescent PDFs, and PDFs that have both red and nonluminescent parts (see also Hamers and Drury 2011). SEM-CL and TEM images of this type of grain are shown in Fig. 4. This grain contains both amorphous PDFs (light in the diffuse dark-field image in Fig. 4b) and PDFs that are planes of high defect density (Fig. 4c). Again, the presence of bright diffuse scattering intensity in the diffraction pattern is consistent with the presence of amorphous material in the sample.

CL Spectra of Red Luminescent PDFs

CL spectra were measured in the SEM in five grains with red luminescent PDFs in a granite fragment from the Ries crater (Fig. 5). The main peaks in the spectra in both PDF and host quartz are at 410 nm and 650 nm, which are commonly occurring peaks in quartz (see the Cathodoluminescence section). After a measurement time of 30 seconds, the intensity ratio of the 650 nm and 410 nm peaks is higher in the PDFs

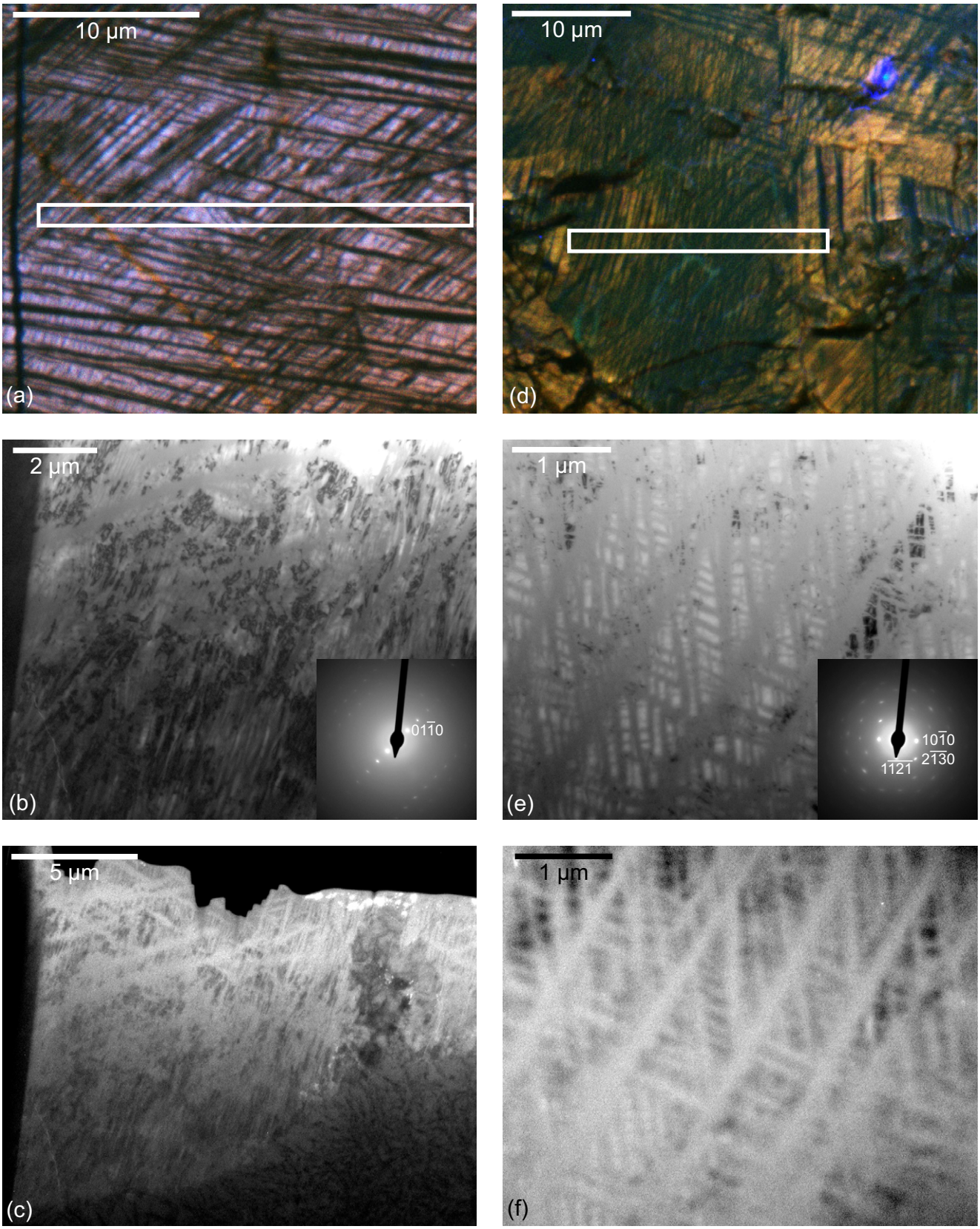
10 μm
(a)
10 μm
(d)
2 μm
$01\bar{1}0$
(b)
1 μm
$10\bar{1}0$
$2\bar{1}30$
$\bar{1}121$
(e)
5 μm
(c)
1 μm
(f)

Fig. 1. Nonluminescent PDFs in a quartz grain in a suevite from the Ries crater (a–c) and experimentally shocked Hospital Hill quartzite (d–f). a) Composite color CL image showing nonluminescent PDFs. The white rectangle shows the location of the TEM foil. b) Bright-field TEM image of part of the foil. Medium gray PDFs are amorphous; in between diffracting (crystalline) material is present. Inset: SADP (selected area diffraction pattern) of PDFs and surrounding material. The bright diffuse scattering disk is consistent with the presence of amorphous material. Slight streaking of the outer diffraction spots indicates the presence of small misorientations in the crystalline material, possibly a microcrystalline grain structure. c) Diffuse dark-field image of the same grain, showing the presence of amorphous (bright) material in the PDFs. d) Composite color CL image showing nonluminescent PDFs. The white rectangle shows the location of the TEM foil. e) Bright-field TEM image of part of the foil. Medium gray PDFs are amorphous; in between diffracting (crystalline) material is present. Inset: SADP of PDFs and surrounding material. The bright diffuse scattering disk is consistent with the presence of amorphous material. Slight streaking of diffraction spots indicates the presence of small misorientations in the crystalline material, possibly a microcrystalline grain structure. f) Diffuse dark-field image of the same grain, showing the presence of amorphous (bright) material in the PDFs.

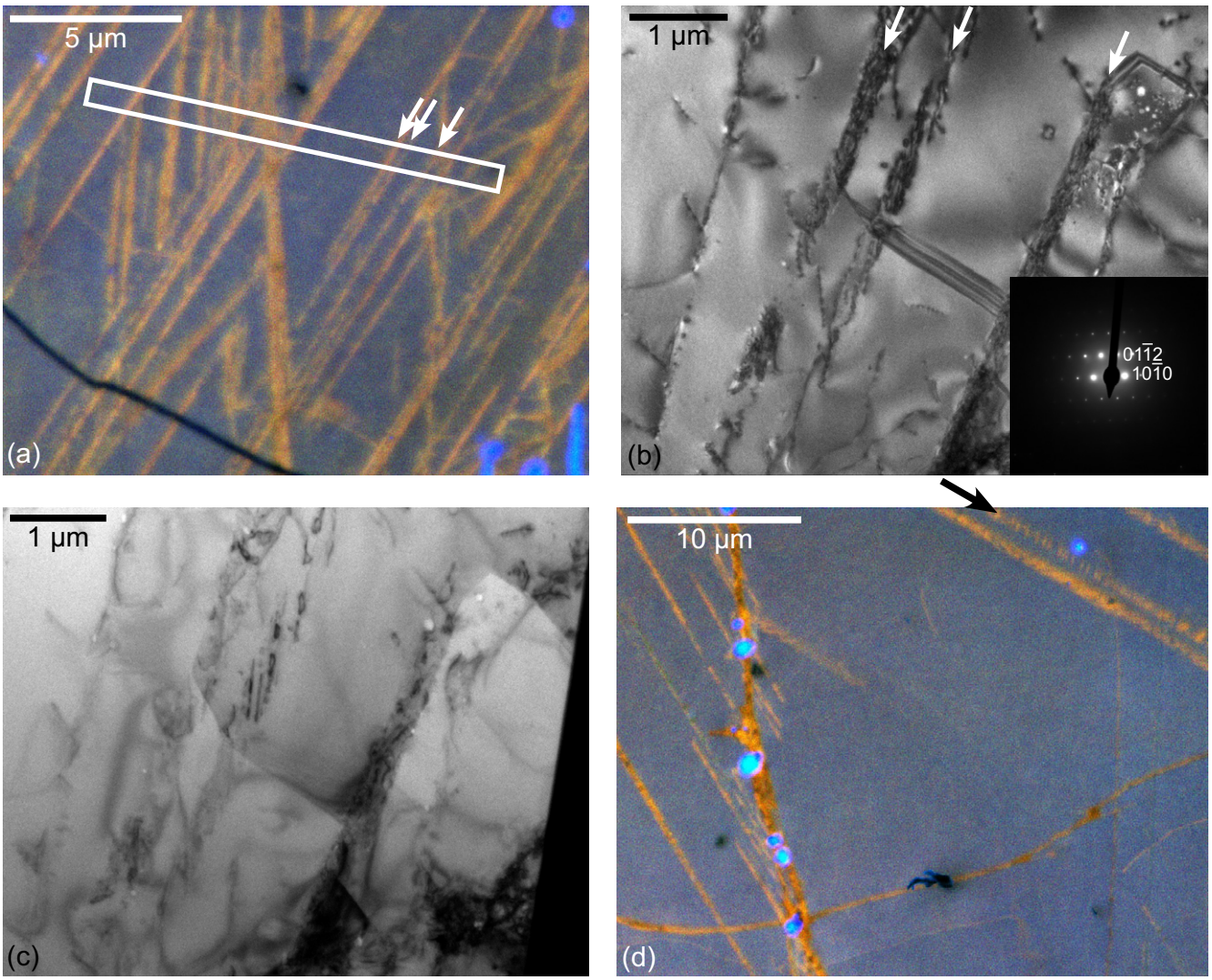

Fig. 2. Red luminescent PDFs in an impact melt rock from Rochechouart (a–c) and a granite fragment from Ries (d). a) Composite color CL image showing at least three orientations of red luminescent PDFs (N–S, NNE–SSW, and ENE–WSW). The white rectangle shows the location of the TEM foil. The three white arrows indicate the three PDFs that are visible in the TEM image shown in (b). b) Bright-field TEM image showing that the PDFs consist of arrays of dislocations. Dauphiné twins are also present, with boundaries partly following the orientation of PDFs. No streaking of diffraction spots occurs (inset), showing the single crystal nature of this grain. The three white arrows indicate the same three PDFs that are indicated in (a). c) Bright-field TEM image of the same area as in (b), tilted to show the Dauphiné twins more clearly. d) Composite color image showing red luminescent PDFs. In the upper right corner are three lamellae consisting of sublamellae that could be arrays of dislocations. This is particularly clear in the central lamella, indicated by the black arrow.

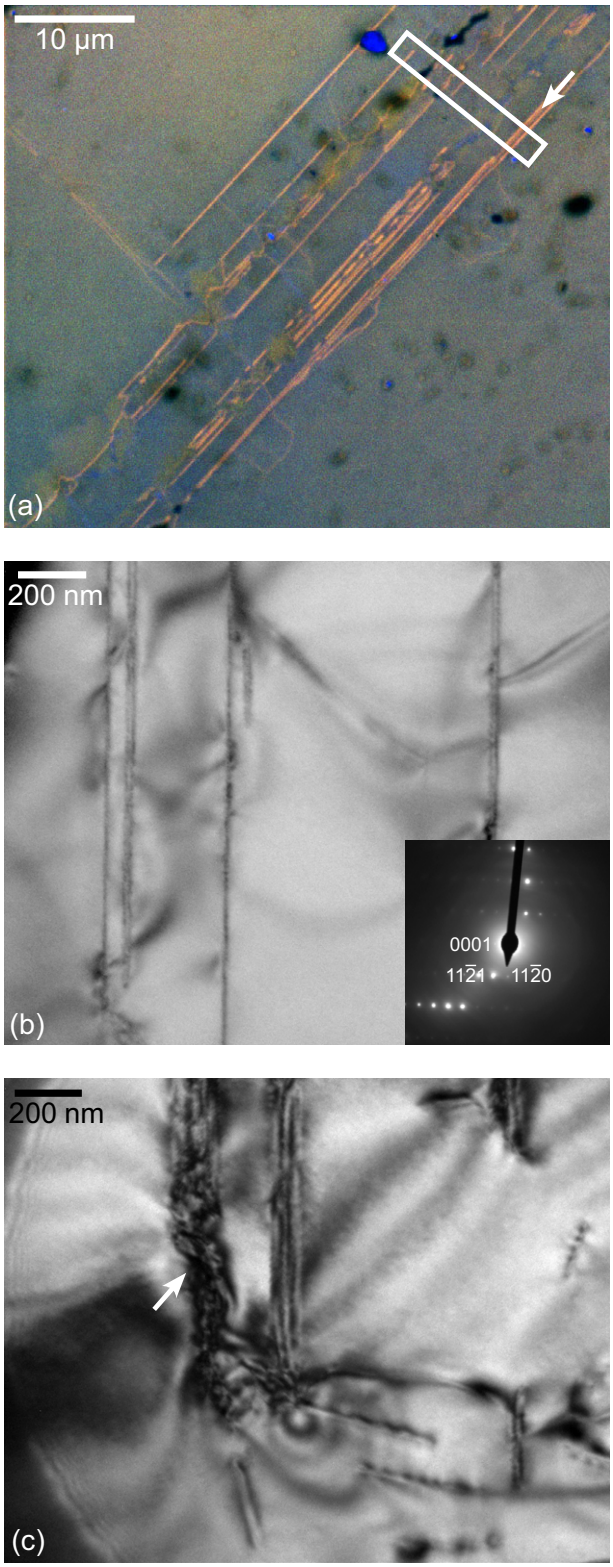

Fig. 3. Red luminescent Brazil twins (Vredefort). a) Composite color CL image showing one set of red luminescent PDFs. The white rectangle shows the location of the TEM foil. The white arrow shows the group of twin boundaries that are shown in the TEM image in (b). b) Bright-field TEM image showing that the PDFs are basal Brazil twins, oriented edge-on. The SADP (inset) shows the Brazil twins are parallel to the basal plane. c) Bright-field TEM image showing the Brazil twins in a tilted position. Parts of the twin plane are decorated by dislocations (white arrow).

than in the host quartz (Fig. 5d). This indicates that the CL spectra of red luminescent PDFs have a stronger 650 nm peak than the surrounding quartz. This is observed in all studied grains. On average, with a measurement time of 30 s, the 650/410 nm peak ratio is 1.7 for PDFs versus 1.3 for the host quartz (Fig. 6); that is, the 650/410 nm peak ratio is 24% higher in PDFs.

The intensity of the red 650 nm peak in quartz increases with increasing irradiation time in the SEM, while the blue 410 nm peak slightly decreases. The intensity increase of the 650 nm emission is quicker in the PDFs than in the host quartz and therefore PDFs are red in CL images. This was also noted by Hamers and Drury (2011), who observed that the red luminescent PDFs become brighter in composite color CL images after scanning the same area several times. This effect can furthermore be observed in Figs. 5a (first scan) and 5b (after several scans): the (panchromatic) CL emission from PDFs is lower than that of the host quartz in the first scan, but brighter in PDFs than in the rest of the grain after several slow scans. The effect can be shown with point measurement times around 30 s, but when longer measurements are taken, the difference between PDFs and host quartz decreases and eventually disappears.

Unfortunately, no peak ratios could be determined for samples with basal Brazil twins (Vredefort), because no areas could be found with a high enough twin density for reliable measurements.

Changes in CL Emission after Prolonged Exposure to the Electron Beam

Figure 7 illustrates the effect of irradiation with the electron beam on the CL emission of quartz. In Figs. 7a and 7b, red squares are areas that have been scanned previously at higher magnification. Prolonged exposure to the electron beam strongly increases the red CL emission of the whole previously scanned area. In Fig. 7b, the central red square is made up of red spots that show where spot measurements were taken for an electron backscattered diffraction (EBSD) map (not discussed in this paper) recorded before scanning the CL image. Figure 7c is a higher magnification scan of the red square on the right in Fig. 7b. In the center of Fig. 7c, another EBSD map was recorded using point

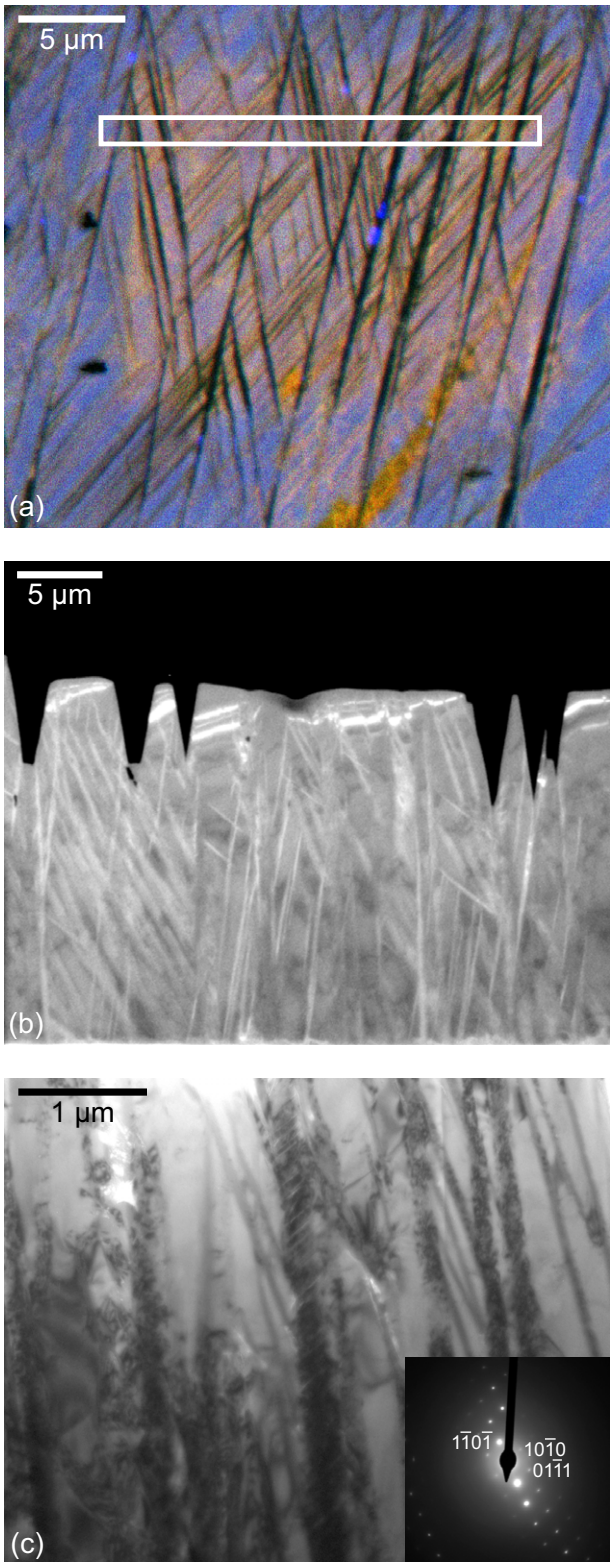

Fig. 4. Red and nonluminescent PDFs (Ries, suevite). a) Composite color CL image showing both red and nonluminescent PDFs. The white rectangle shows the location of the TEM foil. The lighter pinkish square in the center is radiation damage from previous scanning with the electron beam. b) Diffuse dark-field image of the same grain, showing the presence of amorphous (bright) material in some of the PDFs. c) Bright-field TEM image showing both amorphous PDFs and PDFs that are planes of high defect density. No streaking of diffraction spots occurs (inset), indicating that the grain is a single crystal. The PDF in the center (oriented N–S) consists of defects and tiny sublamellae or dislocations.

measurements. The CL emission of the PDFs, which are mostly red luminescent in the rest of the image, has disappeared in the area that has suffered long exposure to the beam during point mapping: the PDFs have become nonluminescent. This effect is also observed in Fig. 7a in a small rectangular area in the top right of the image, indicated by the black arrow. Quenching of the CL emission was not observed as a result of scanning images (even after repeated slow scanning). The CL emission quenched only in sample areas on which the beam was stationary for a relatively long time (~0.2 s on each point in this case, whereas in scanned images, the dwell time was four orders of magnitude lower, typically 30–60 μs per pixel) and with higher voltages and beam currents (20 kV and 2.4 nA for these two examples) than those used for CL imaging.

PDFs Filled with a Blue Luminescent Material

Figure 8 shows backscattered electron (BSE), secondary electron (SE), and composite color SEM-CL images of a quartz grain that was shocked experimentally to 24 GPa. Most of the PDFs in Fig. 8a are darker (less dense) than the surrounding quartz, as is commonly observed in BSE images of shocked quartz grains (e.g., Stähle et al. 2008; Ebert et al. 2013), because PDFs are filled with amorphous SiO_2 that is less dense than crystalline quartz. However, some PDFs in Fig. 8a are filled with a bright material. With EDX measurements of different parts of the grain, both PDFs and host quartz, only the presence of SiO_2 was detected (one spectrum is shown in Fig. 8b), indicating that any chemical differences must be very small and are unlikely to be big enough to account for the strong contrast observed in the BSE image. The BSE contrast in Fig. 8a is therefore likely to be from density differences and unlikely to be from atomic number contrast. Thus, darker shades of gray in the BSE image mean low-density material, while lighter shades of gray indicate higher densities.

Figures 8c and 8d, respectively, show an SE and composite color SEM-CL image of the same grain as is shown in Fig. 8a. Due to an extra polish that was applied to the sample between the SE/CL imaging and the BSE imaging, exact correlation of the PDFs between BSE and SE/CL is not possible, because a thin

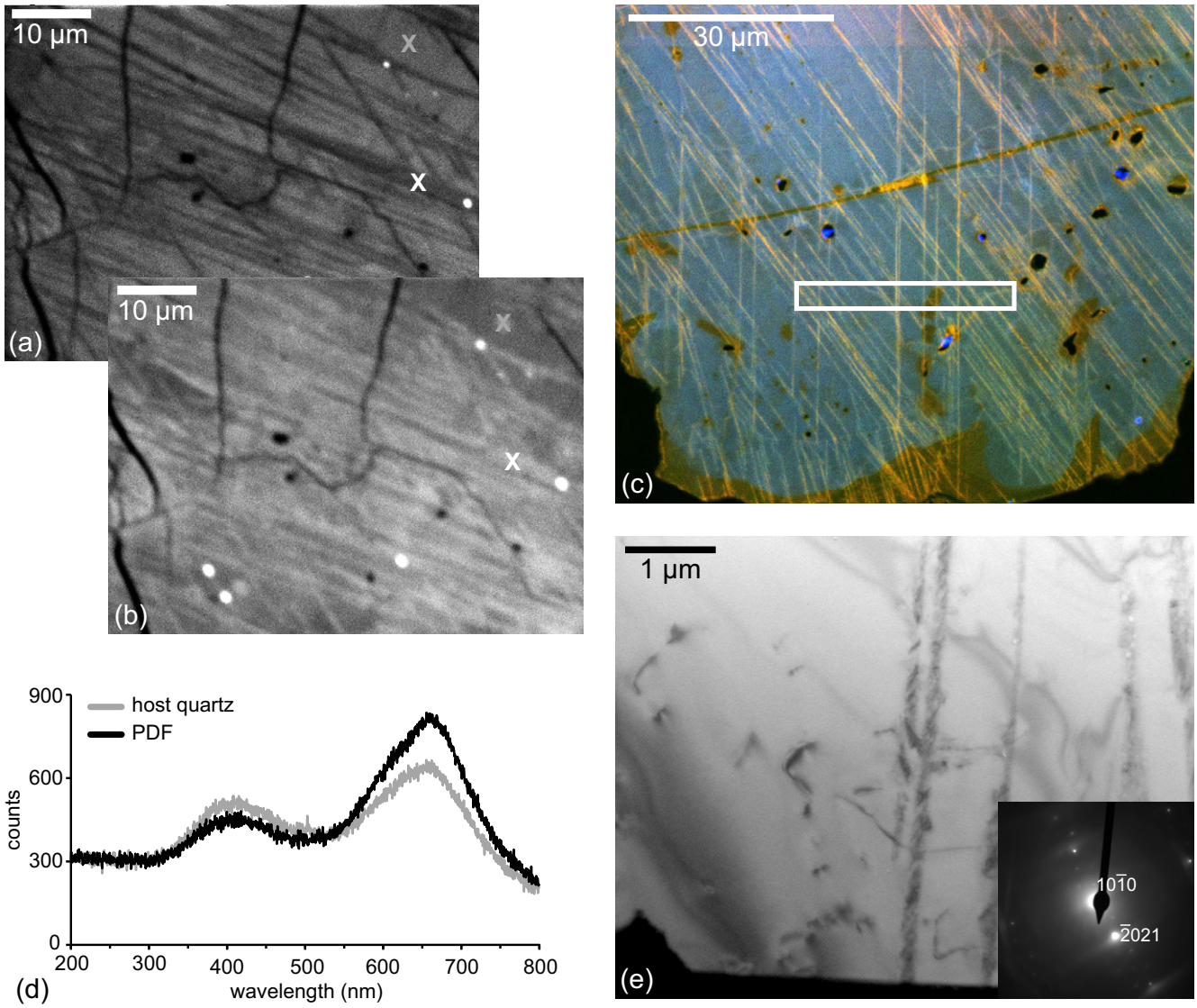

Fig. 5. CL spectroscopic measurements of red luminescent PDFs in a granite fragment from Ries. a) Panchromatic CL image showing multiple sets of PDFs (dark), first scan. b) Same area as in (a), after repeated scanning with the electron beam, showing the increased intensity of the CL emission from the PDFs (now brighter than in [a]). c) Composite color CL image of a different grain from the same thin section showing multiple sets of red luminescent PDFs. The white rectangle shows the location of the TEM foil shown in (e). d) CL spectra of an area with a high density of PDFs (black line; white cross in [a] and [b]) and host quartz (gray line; gray cross in [a] and [b]). The 650 nm peak is higher in the PDFs than in the host quartz. e) Bright-field TEM image of the grain shown in (c), showing that the red luminescent PDFs consist of arrays of dislocations.

layer (a few microns) of the sample surface was removed. However, the PDFs in the SE image show the same characteristics as in the BSE image: some (parts of) PDFs are brighter. Although SE images are commonly used to show topography, also density or phase contrast can be imaged when acceleration voltages above ~5 kV are used, mainly because backscattered electrons excite some secondary electrons on their trajectories out of the surface layer (e.g., Reimer and Hawkes 1998). The density contrast might be enhanced by our use of an Everhart–Thornley detector (Everhart and Thornley 1960), which inevitably detects some backscattered electrons in addition to the secondary electrons. Furthermore, the higher density material could be more resistant to polishing and therefore induce slight topography on the sample surface, enhancing the visibility of the brighter material in the SE image even more.

When comparing the SE image to the composite color SEM-CL image in Fig. 8d, the brighter SE regions clearly show blue luminescence, in contrast to the majority of PDFs, which are nonluminescent.

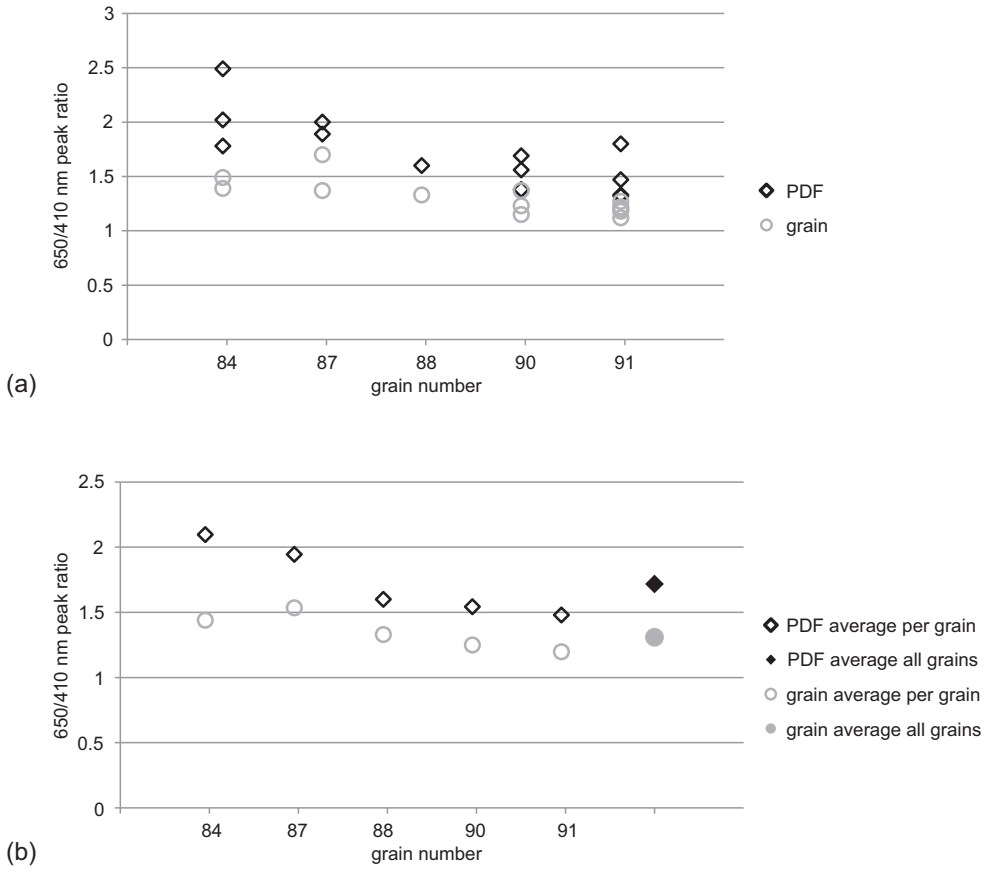

Fig. 6. Plots of the 650/410 nm peak ratios show that the 650 peak is stronger in PDFs than in the host quartz. a) The 650/410 nm peak ratios of PDFs and host quartz; all measurements shown per grain. b) Average 650/410 nm peak ratios of PDFs and host quartz shown per grain and as an average of all measurements.

DISCUSSION

Cathodoluminescence of PDFs

Our results show that the SEM-CL behavior of PDFs in quartz can be directly related to the microstructure of the PDFs as observed in the TEM.

Red Luminescent PDFs

The one-to-one correspondence of SEM-CL and TEM images (Fig. 2) confirms that red luminescence occurs in healed PDFs and is related to the high dislocation density in the PDF plane. The dominant emission peak in red luminescent PDFs is at 650 nm (Figs. 5 and 6), and is therefore related to the nonbridging oxygen hole center, or NBOHC (see the Cathodoluminescence section) (Stevens Kalceff and Phillips 1995; Stevens Kalceff et al. 2000; Götze et al. 2001).

The NBOHC defect ($O_3{\equiv}Si\text{-}O$) can be induced under electron irradiation by dissociation of a (strained) Si-O bond by radiolysis (an effect known to microscopists as "beam damage"). Radiolysis is a process in which atoms are displaced by inelastic interactions of the electron beam with the sample. It occurs in quartz at beam energies above ~5 kV (Stevens Kalceff et al. 2000; Stevens Kalceff 2009). The 650 nm CL emission associated with dissociation of a Si-O bond increases with increasing scanning time and then stabilizes (Stevens Kalceff et al. 2000; Götze et al. 2001). Two other important precursors for the NBOHC are $O_3{\equiv}Si\text{-}O\text{-}H$, where electron irradiation breaks the O-H bond, and $O_3{\equiv}Si\text{-}O\text{-}M$, where M is an alkali ion and electron irradiation dissociates the O-M bond. However, the CL emission associated with these two precursors is quickly quenched (Götze et al. 2001; Stevens Kalceff 2009). Furthermore, peroxy linkages (Si-O-O-Si) are often mentioned as a precursor defect for the NBOHC (Stevens Kalceff and Phillips 1995; Stevens Kalceff et al. 2000; Götze et al. 2001).

The CL emission of the red luminescent, healed PDFs shows an increase with increasing irradiation time (see fig. 7 and Hamers and Drury 2011). This suggests that the NBOHC induced by Si-O bond dissociation by

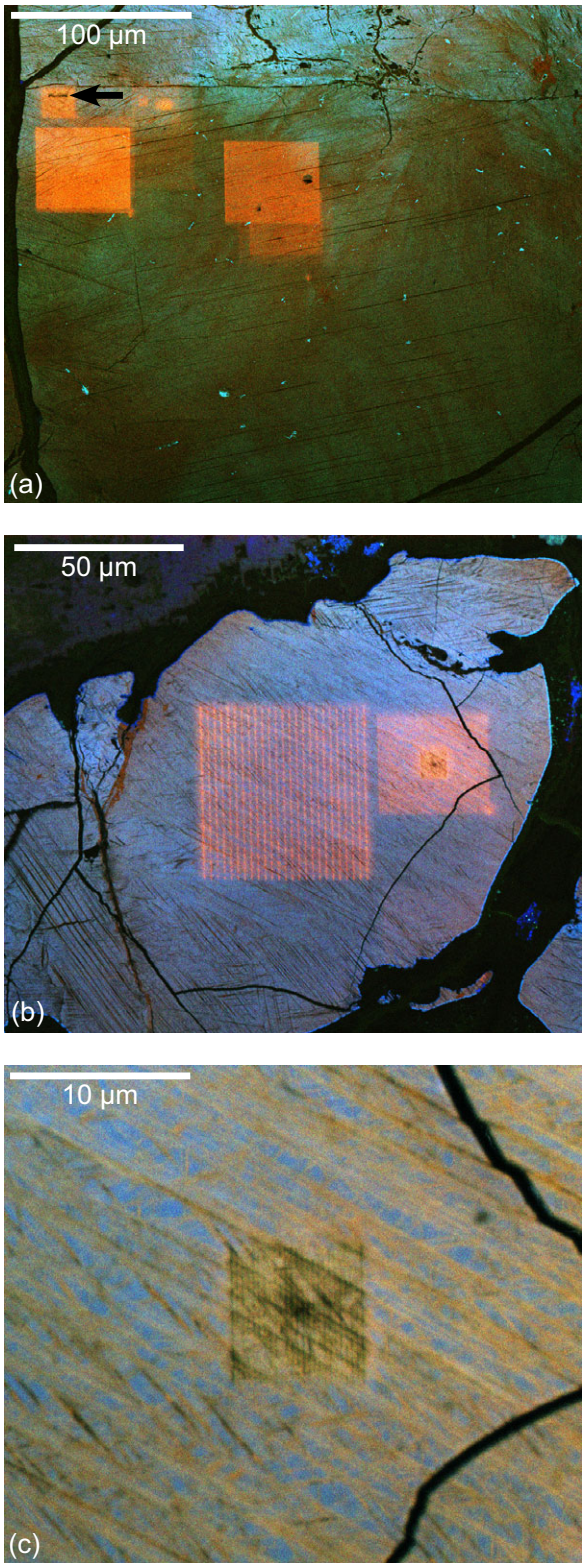

Fig. 7. Composite color images of grains in a granite fragment from the Ries crater. a) Low magnification image showing red squares where higher magnification images have been scanned before at a slow scanning rate. A small rectangle has become completely nonluminescent after intense spot irradiation due to point measurements for an EBSD map (top left, black arrow). b) Low magnification image showing red squares where higher magnification images have been scanned before at a slow scanning rate (right) and where an EBSD map was recorded using point measurements (center). c) Higher magnification image of the red square on the right in (c). The square in the center shows changes in CL emission of the part of the sample where point measurements have been taken for EBSD mapping. The PDFs in the square, which are mostly red in the rest of the image, have become nonluminescent.

radiolytic beam damage processes is the main source for the red CL emission. This production of NBOHC defects accompanied by red CL emission is a well-known phenomenon and also takes place in undamaged crystalline quartz (e.g., Stevens Kalceff and Phillips 1995; Götze et al. 2001; Stevens Kalceff 2009)—as can also be observed in Fig. 7, where previously scanned areas even without PDFs show a strong red CL emission. However, PDFs are quicker to show effects of irradiation damage than the surrounding quartz, and to show an increasingly bright red luminescence. In TEM, localized electron beam damage, mainly by radiolytic processes, is a commonly observed phenomenon at dislocations, fluid inclusions, and twin boundaries, where continued beam damage finally results in complete (local) amorphization (McLaren et al. 1970; Comer 1972; Cherns et al. 1980; Carter and Kohlstedt 1981). The combination of the red CL emission at 650 nm with strongly increasing intensity in PDFs, the high dislocation density along healed PDFs in TEM, and the known phenomenon of localized beam damage in TEM at defects strongly suggest that preferential electron beam damage at dislocations produces NBOHC defects by breaking Si-O bonds, forming the source of the red luminescence in healed PDFs. In rare cases, even individual dislocations within the healed PDFs are apparently detected in SEM-CL images, as is shown by the PDFs in the upper right corner of Fig. 2d. These PDFs consist of arrays of tiny red luminescent "sublamellae" that look similar to the arrays of dislocations observed in healed PDFs in TEM (e.g., Figs. 2b and 2c, and figures in Goltrant et al. [1991] and Trepmann and Spray [2006]).

The presence of OH bonds may also play a role in the production of NBOHC defects and the related red CL emission. Healed PDFs are thought to form by water-assisted crystallization of the initially amorphous PDFs under high postshock temperatures or metamorphic events (Grieve et al. 1996), so obviously water must be present in healed PDFs. This is supported by the fluid inclusions that usually decorate healed PDFs (Goltrant et al. 1992; Grieve et al. 1996). As OH groups may preferentially bond to nonbridging atoms in dislocation cores (e.g., Trepied and Doukhan

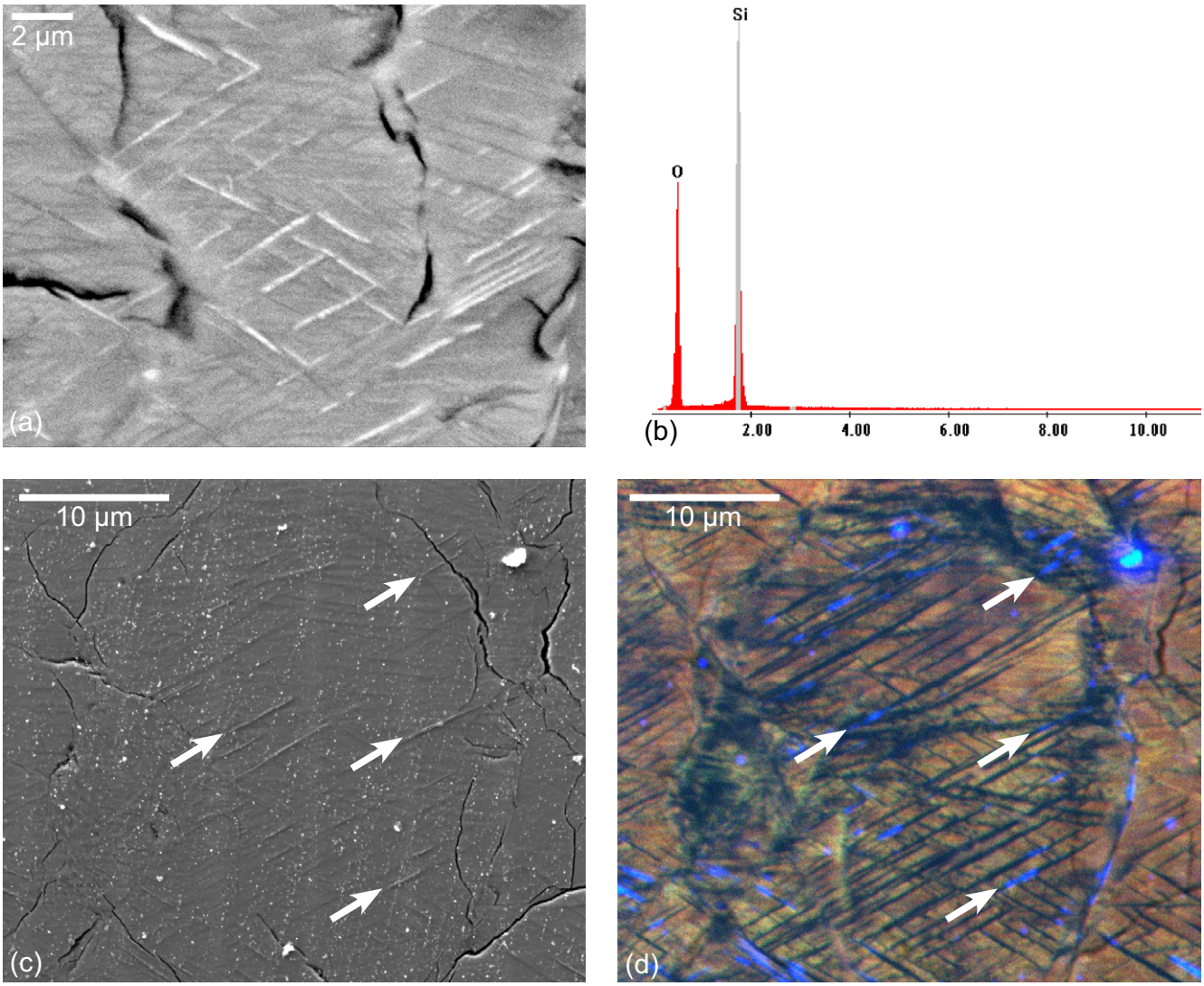

Fig. 8. Experimentally shocked single crystal quartz. a) BSE image, clearly showing that some PDFs are filled with denser (brighter) material. b) The EDX spectrum from the brighter material shows that it has SiO_2 composition. c) SE image of the same grain as in (a) (lower magnification), showing some density contrast as well as topography. White arrows indicate some clear examples of PDFs that are denser (brighter). Although the density component in the SE contrast is not as strong as in BSE images, it can be observed in this grain (recorded with an acceleration voltage of 5 kV and a beam current of 1.6 nA). The bright areas do not correspond exactly with those in the BSE image in (c), because the grain has been polished in between imaging (c/d) and (a), but the geometry of the denser material is the same. d) Composite color SEM-CL image of the same area as shown in (c). White arrows indicate the same PDFs filled with a denser material as in (c), that are brighter in the SE image. The denser material shows blue luminescence.

1978; Heggie 1992), it is likely that a relatively high concentration of OH groups are present in healed PDFs and that these (at least initially) contribute to the red luminescence. To check the presence of OH groups in healed PDFs, micro-Raman spectroscopy could be applied in a future study.

Not only healed PDFs but also Brazil twins are red luminescent in SEM-CL images (Fig. 3). If dislocations are present along the twin plane, they could be a source of the red luminescence, but more likely the red CL emission comes also from the twin plane itself, because the dislocation density in the Brazil twin plane is usually much lower than in healed PDFs and large parts of the twin plane are free of dislocations (Fig. 3). Furthermore, McLaren and Phakey (1965) observed very quick preferential damage along Brazil twin boundaries in amethyst in TEM, similar to the damage occurring at dislocations. The necessary precursors for the NBOHC may be strained bonds in the locally distorted tetrahedral structure in the twin boundary, or alternatively OH groups, peroxy linkages, or impurities along the twin boundary.

Nonluminescent PDFs

Figure 1 shows that nonluminescent PDFs contain amorphous material. Although the 650 nm CL emission is a commonly observed peak in fused (low pressure, high temperature produced) silica glass, i.e., amorphous silica (Stevens Kalceff et al. 2000; Fitting et al. 2001), in the amorphous material in nonluminescent PDFs, such as the grain from the Ries crater and the experimentally shocked grain in Fig. 1, the structure is apparently so damaged and disordered that no CL emission is possible. Due to the extreme pressures and temperatures involved in impact processes, the crystal structure in PDFs formed at high pressure could be completely destroyed, preventing any photon emission under electron bombardment. The conclusion that the material in nonluminescent PDFs is amorphous is supported by our observations of the effect of beam damage on the CL emission of quartz. Figure 7 shows that prolonged intense electron irradiation, with the beam in spot mode, first induces an increase in red CL emission, but finally results in nonluminescence. This suggests that ongoing beam damage eliminates all luminescence centers. As damage processes in TEM and SEM are largely the same and beam damage in TEM finally results in local amorphization, it is likely that the same happens in SEM and that localized amorphization is observed as localized quenching of CL emission.

An alternative explanation for the nonluminescence of amorphous PDFs might be variations in trace element concentrations, for example iron content. Although interstitial Fe^{3+} in (crystalline) quartz is mentioned as the source of a red luminescence peak around 700-750 nm (Götze 2009; Stevens Kalceff 2009), it has also been suggested that the presence of iron can quench other CL emissions (Haddad et al. 2006). Chemical analysis of experimentally shocked quartz grains suggests that grains with a high density of PDFs contain an increased amount of metals from the iron meteorite projectile that was involved (Ebert et al. 2013). If meteoritic iron, or iron from another source, is in some way distributed preferentially into the PDFs, it could quench the luminescence. In this context, it would be interesting in a future study to map the trace element distribution in shocked quartz grains with nonluminescent amorphous PDFs.

The breaking of Si-O bonds due to electron irradiation is in fact very local amorphization in the direct vicinity of the defect. Because defects in SiO_2 disturb the short-range order, the defect structure and most luminescence centers in crystalline and amorphous SiO_2 are similar (Sigel and Marrone 1981; Stevens Kalceff and Phillips 1995; Stevens Kalceff 2013). It has even been suggested that the NBOHC and most other defects in quartz are associated with locally amorphous parts of the crystal structure (Stevens Kalceff 2009, 2013). Furthermore, as mentioned earlier, the 650 nm peak is a commonly observed CL emission in fused SiO_2 glass (Stevens Kalceff et al. 2000; Fitting et al. 2001; Stevens Kalceff 2013). It is therefore theoretically possible that some amorphous PDFs are red luminescent. However, red luminescent amorphous PDFs were not observed in our samples. Apparently, the structure or trace element composition of amorphous PDFs is not the same as that of most types of fused silica glass.

It is worth noting, as was already reported by Hamers and Drury (2011), that only highly shocked grains were observed with exclusively nonluminescent PDFs. In these grains, the PDFs are always thick and slightly wavy and irregularly shaped: the characteristics of PDFs formed at high shock pressures > 25 GPa (Langenhorst 1994). No grains were observed with only nonluminescent PDFs showing characteristics of a lower shock stage (i.e., fewer sets, more widely spaced and thin and straight PDFs). Even in relatively recent structures, such as the 3.6 Ma El'gygytgyn crater (images not shown), grains with characteristics of lower shock pressure and with only nonluminescent PDFs were not observed. The most probable explanation for the apparent lack of moderately shocked quartz grains with exclusively nonluminescent PDFs is that, even in relatively recent impact structures, a significant proportion of the amorphous material has crystallized and many (parts of) PDFs are healed. Under similar temperature conditions, thinner PDFs, formed at lower shock pressures, will likely heal more easily than wider PDFs, which formed at much higher shock pressures.

Several other explanations for the lack of moderately shocked grains with nonluminescent PDFs might be considered: A) amorphous PDFs in grains shocked to lower pressures are too narrow to be detected as nonluminescent in CL images, but instead defects or damage zones along the PDFs give rise to a red luminescent signal; B) unaltered PDFs at lower shock stages are not (completely) amorphous; C) lower shock amorphous PDFs contain amorphous material with a different structure, that is red instead of nonluminescent —in this case, these PDFs would be indistinguishable from healed ones in the CL images in this study. Scenario A is unlikely, as thin and straight, but nonluminescent and amorphous PDFs were observed in the grain in Fig. 4. No direct evidence for scenarios B or C can be found in our data, but from the literature and our results, it is clear that amorphous SiO_2 can exhibit different types of CL behavior. TEM and SEM-CL observations on very recent or, preferably, experimentally shocked quartz should be able to solve this issue.

Besides TEM analysis, also (micro-)Raman spectroscopy could help in determining the presence of

amorphous material in PDFs and the structural configuration of the crystal lattice in shocked quartz grains. Gucsik et al. (2011) and Pittarello et al. (2015) showed promising results using this technique on shocked quartz from the Ries crater and the El'Gygytgyn impact structure, respectively. A future combination of CL and Raman analyses of shocked quartz (e.g., similar to the methods used by Okumura et al. [2009] on ballen silica) might provide more information on the characteristics of the amorphous material in nonluminescent PDFs.

Blue Luminescent High-Pressure Phase

In the experimentally shocked quartz grain in Fig. 8, PDFs were observed filled with a material that is bright in BSE images and blue luminescent in CL images. Because the material is brighter than the host quartz in BSE images, it must have a higher density, but with EDX spectra only SiO_2 was detected in both the bright material and the host grain. Therefore, the bright material can be interpreted as a high-pressure SiO_2 phase. Two high-pressure polymorphs of quartz are frequently observed in impact environments: coesite and stishovite (e.g., Stöffler and Langenhorst 1994; Stähle et al. 2008). Stishovite is estimated to occur in quartz shocked to pressures between ~12 and 45 GPa, while coesite only appears at pressures above ~30 GPa (Stöffler and Langenhorst 1994). The grain in Fig. 8 was shocked to 24 GPa, which is in the pressure range in which stishovite can form. Furthermore, the high-density phase has the same geometry and appearance as the stishovite-filled PDFs shown by Stähle et al. (2008) in their fig. 2. The blue CL is also consistent with stishovite: Fitting et al. (2001) showed that the CL emission of stishovite from Barringer Crater (Arizona, USA) at room temperature has a broad band that is a combination of peaks around 420, 460, and 500 nm. Trukhin et al. (2003, 2014) also observed a blue luminescence band in stishovite. Because of the shock pressure, geometry, and CL emission color, the high-pressure phase observed in the grain in Fig. 8 can be interpreted as stishovite. Alternatively, as it is unknown whether this high-density phase is crystalline or not, it could be a high-pressure amorphous form of SiO_2.

The observation of the blue luminescent high-density phase in Fig. 8 illustrates that, like BSE images, composite color SEM-CL imaging can be used as an indication for the presence of high-pressure phases in shocked quartz. However, care should be taken with a definitive interpretation, because remains of polishing material or dust particles on the sample surface can also be blue luminescent (see the bright blue spots present in most color CL images in this paper and fig. 4 in Hamers and Drury 2011), as might possible secondary minerals in altered rocks. Chemical analysis of the composition of the phase and TEM or EBSD observations, providing information on crystal structure, would be required to confirm the nature of a potential high-pressure form of SiO_2.

Use of SEM-CL Imaging as Evidence for Impact Structures

Although above results show that SEM-CL imaging is a very useful technique to identify and characterize PDFs in quartz, it does not provide a quick and easy "short-cut" to prove the shock origin of planar microstructures in quartz. Also deformation lamellae can be imaged with this technique and even though in high quality images PDFs can be distinguished from nonimpact-related planar or subplanar microstructures (Hamers and Drury 2011), this is not a quantitative method. To obtain the best possible SEM-CL images, good sample preparation and a carbon coat as thin as possible are essential, in order to obtain the strongest signal (see Frelinger et al. [2015] for a detailed discussion on recording high-quality SEM-CL images). Higher beam currents increase signal strength, but reduce spatial resolution. Slower scanning times strongly increase image quality, but also beam damage effects.

If a researcher aims to identify shocked quartz to provide evidence for a new impact structure, it remains important to start with proper light microscopy studies to identify potentially shocked grains, study as many grains as possible, and to use multiple methods to cross-check any evidence. Additional methods that could be used are universal stage measurements of PDF orientation distributions (made much easier by recent work of Ferrière et al. 2009; Huber et al. 2011; and Losiak et al. 2016) and TEM analysis (e.g., Goltrant et al. 1991, 1992; Langenhorst 1994, 1996; Trepmann and Spray 2006). Also Raman spectroscopy (e.g., Gucsik et al. 2011), EBSD, and other SEM techniques, and chemical analyses like EDX and WDS can provide useful information.

CONCLUSIONS

The combination of color SEM-CL imaging and TEM analysis of shocked quartz grains confirms the great potential of color SEM-CL imaging as a method to identify PDFs in quartz, and also illustrates the complexities that are involved in interpreting CL emissions, especially in images. A very useful result of this study for crater research is that color SEM-CL imaging can distinguish between fresh (amorphous) and healed PDFs or basal Brazil twins: nonluminescent PDFs are amorphous, while healed PDFs and basal

Brazil twins are red luminescent. TEM and CL spectrometry confirm that the dominant peak in the emission from red luminescent PDFs is around 650 nm, related to the NBOHC, and is most likely the result of preferential beam damage at dislocations and twin boundaries. A high-pressure phase, possibly stishovite, can be detected in color SEM-CL images as blue luminescent parts of PDFs. Although not all details of the CL emission of PDFs can be explained at this time, SEM-CL imaging is a great method to visualize subtle differences in shock microstructures in quartz. For more quantitative information, additional analysis can be done on the same samples using other techniques, such as TEM, EBSD, or light microscopy with universal stage for crystallographic orientations of grains or PDFs, Raman spectroscopy for extra information on amorphous material and crystal order, and EDX/WDS mapping or CL spectroscopy for defect and trace element distributions.

Acknowledgments—Uwe Reimold, Uli Raschke, and Jörg Fritz are thanked for kindly providing experimentally shocked and El'gygytgyn samples; Roald Tagle for Popigai samples; and Rodger Hart for Vredefort samples. Pim van Wamel has been of great help during sampling at the Ries crater, and Philippe Lambert at Rochechouart. We thank Gordon Osinski for editorial handling and Gordon Osinski and Arnold Gucsik for their helpful and constructive comments on the study. This study was funded by NWO, the Netherlands Organization for Scientific Research.

Editorial Handling—Dr. Gordon Osinski

REFERENCES

Boggs S., Krinsley D. H., Goles G. G., Seyedolali A., and Dypvik H. 2001. Identification of shocked quartz by scanning cathodoluminescence imaging. *Meteoritics & Planetary Science* 36:783–791.

Carter C. B. and Kohlstedt D. L. 1981. Electron irradiation damage in natural quartz grains. *Physics and Chemistry of Minerals* 7:110–116.

Cherns D., Hutchison J. L., Jenkins M. L., Hirsch P. B., and White S. 1980. Electron irradiation induced vitrification at dislocations in quartz. *Nature* 287:314–316.

Christie J. M. and Ardell A. J. 1974. Substructures of deformation lamellae in quartz. *Geology* 2:405–408.

Christie J. M. and Raleigh C. B. 1959. The origin of deformation lamellae in quartz. *American Journal of Science* 257:385–407.

Comer J. J. 1972. Electron microscope study of dauphiné microtwins formed in synthetic quartz. *Journal of Crystal Growth* 15:179–187.

Cordier P. and Gratz A. J. 1995. TEM study of shock metamorphism in quartz from the Sedan nuclear test site. *Earth and Planetary Science Letters* 129:163–170.

Drouin D., Couture A. R., Joly D., Tastet X., Aimez V., and Gauvin R. 2007. CASINO V2.42—A fast and easy-to-use modeling tool for scanning electron microscopy and microanalysis users. *Scanning* 29:92–101.

Drury M. R. 1993. Deformation lamellae in metals and minerals. In *Defects and processes in the solid state: Geoscience applications*, edited by Boland J. N. and Fitz Gerald J. D. Amsterdam: Elsevier Science Publishers B. V. pp. 195–212.

Ebert M., Hecht L., Deutsch A., and Kenkmann T. 2013. Chemical modification of projectile residues and target material in a MEMIN cratering experiment. *Meteoritics & Planetary Science* 48:134–149.

Engelhardt W. von and Bertsch W. 1969. Shock induced planar deformation structures in quartz from the Ries crater, Germany. *Contributions to Mineralogy and Petrology* 20: 203–234.

Everhart T. E. and Thornley R. F. M. 1960. Wide-band detector for micro-microampere low-energy electron currents. *Journal of Scientific Instruments* 37:246.

Ferrière L., Morrow J. R., Amgaa T., and Koeberl C. 2009. Systematic study of universal-stage measurements of planar deformation features in shocked quartz: Implications for statistical significance and representation of results. *Meteoritics & Planetary Science* 44:925–940.

Fitting H.-J., Barfels T., Trukhin A. N., and Schmidt B. 2001. Cathodoluminescence of crystalline and amorphous SiO_2 and GeO_2. *Journal of Non-Crystalline Solids* 279: 51–59.

Frelinger S. N., Ledvina M. D., Kyle J. R., and Zhao D. 2015. Scanning electron microscopy cathodoluminescence of quartz: Principles, techniques and applications in ore geology. *Ore Geology Reviews* 65:840–852.

French B. M. and Koeberl C. 2010. The convincing identification of terrestrial meteorite impact structures: What works, what doesn't, and why. *Earth-Science Reviews* 98:123–170.

French B. M., and Short N. M. 1968. Shock metamorphism of natural materials: Proceedings of the First Conference Held at NASA, Goddard Space Flight Center, Greenbelt, Maryland, April 14-16, 1966. Baltimore, Maryland: Mono Book Corp.

Fritz J., Wünnemann K., Reimold W. U., Meyer C., and Hornemann U. 2011. Shock experiments on quartz targets pre-cooled to 77 K. *International Journal of Impact Engineering* 38:440–445.

Goltrant O., Cordier P., and Doukhan J.-C. 1991. Planar deformation features in shocked quartz; a transmission electron microscopy investigation. *Earth and Planetary Science Letters* 106:103–115.

Goltrant O., Leroux H., Doukhan J.-C., and Cordier P. 1992. Formation mechanisms of planar deformation features in naturally shocked quartz. *Physics of the Earth and Planetary Interiors* 74:219–240.

Götte T. 2009. Petrological modifications in continental target rocks from terrestrial impact structures: Evidence from cathodoluminescence. In *Cathodoluminescence and its application in the planetary sciences*, edited by Gucsik A. Berlin: Springer. pp. 45–60.

Götze J. 2009. Chemistry, textures and physical properties of quartz—Geological interpretation and technical application. *Mineralogical Magazine* 73:645–671.

Götze J., Plötze M., and Habermann D. 2001. Origin, spectral characteristics and practical applications of the cathodo-

luminescence (CL) of quartz—A review. *Mineralogy and Petrology* 71:225–250.

Grieve R. A. F., Langenhorst F., and Stöffler D. 1996. Shock metamorphism of quartz in nature and experiment: II. Significance in geoscience. *Meteoritics & Planetary Science* 31:6–35.

Gucsik A., Okumura T., Kayama M., Nishido H., and Ninagawa K. 2011. Planar deformation features in quartz from the Ries impact crater: Advanced by micro-Raman spectroscopy. *Spectroscopy Letters* 44:469–473.

Gucsik A., Okumura T., Nishido H., Gyollai I., Ninagawa K., Deseta N., and Rózsa P. 2015. Non-luminescent nature of the planar deformation features in shocked quartz from the Ries impact structure, Germany: A new interpretation. *Central European Geology* 58:217–229.

Haddad S. C., Worden R. H., Prior D. J., and Smalley P. C. 2006. Quartz cement in the Fontainebleau sandstone, Paris Basin, France: Crystallography and implications for mechanisms of cement growth. *Journal of Sedimentary Research* 76:244–256.

Hamers M. F. and Drury M. R. 2011. Scanning electron microscope-cathodoluminescence (SEM-CL) imaging of planar deformation features and tectonic deformation lamellae in quartz. *Meteoritics & Planetary Science* 46:1814–1831.

Heggie M. I. 1992. A molecular water pump in quartz dislocations. *Nature* 355:337–339.

Huber M. S., Ferrière L., Losiak A., and Koeberl C. 2011. ANIE: A mathematical algorithm for automated indexing of planar deformation features in quartz grains. *Meteoritics & Planetary Science* 46:1418–1424.

Lana S. L. B. and Seddon A. B. 1998. X-Ray diffraction studies of sol-gel derived ORMOSILs based on combinations of tetramethoxysilane and trimethoxysilane. *Journal of Sol-Gel Science and Technology* 13:461–466.

Langenhorst F. 1994. Shock experiments on pre-heated alpha-quartz and beta-quartz: II. X-ray and TEM investigations. *Earth and Planetary Science Letters* 128:683–698.

Langenhorst F. 1996. Characteristics of shocked quartz in late Eocene impact ejecta from Massignano (Ancona, Italy): Clues to shock conditions and source crater. *Geology* 2:487–490.

Losiak A., Golebiowska I., Ferrière L., Wojciechowski J., Huber M. S., and Koeberl C. 2016. WIP: A Web-based program for indexing planar features in quartz grains and its usage. *Meteoritics & Planetary Science* 51:647–662.

Marshall D. J. 1988. *Cathodoluminescence of geological materials*. Boston: Unwin Hyman. 146 p.

McLaren A. and Phakey P. P. 1965. A transmission electron microscope study of amethyst and citrine. *Australian Journal of Physics* 18:135–141.

McLaren A. C., Turner R. G., Boland J. N., and Hobbs B. E. 1970. Dislocation structure of the deformation lamellae in synthetic quartz; a study by electron and optical microscopy. *Contributions to Mineralogy and Petrology* 29:104–115.

Okumura T., Gucsik A., Nishido H., Ninagawa K., and Toyoda S. 2009. Cathodoluminescence microcharacterization of ballen silica in impactites. *AIP Conference Proceedings* 1163:148–154.

Perny B., Eberhardt P., Ramseyer K., Mullis J., and Pankrath R. 1992. Microdistribution of Al, Li, and Na in alpha quartz; possible causes and correlation with short-lived cathodoluminescence. *American Mineralogist* 77:534–544.

Pittarello L., Roszjar J., Mader D., Debaille V., Claeys P., and Koeberl C. 2015. Cathodoluminescence as a tool to discriminate impact melt, shocked and unshocked volcanics: A case study of samples from the El'gygytgyn impact structure. *Meteoritics & Planetary Science* 50:1954–1969.

Ramseyer K. and Mullis J. 1990. Factors influencing the short-lived blue cathodoluminescence of alpha-quartz. *Amarican Mineralogist* 75:791–800.

Ramseyer K. and Mullis J. 2000. Geologic application of cathodoluminescence in silicates. In *Cathodoluminescence in geosciences*, edited by Pagel M., Barbin V., Blanc P., and Ohnenstetter D. Berlin: Springer. pp. 177–191.

Ramseyer K., Aldahan A. A., Collini B., and Landström O. 1992. Petrological modifications in granitic rocks from the Siljan impact structure: Evidence from cathodoluminescence. *Tectonophysics* 216:195–204.

Raschke U., Schmitt R. T., and Reimold W. U. 2013. Petrography and geochemistry of impactites and volcanic bedrock in the ICDP drill core D1c from Lake El'gygytgyn, NE Russia. *Meteoritics & Planetary Science* 48:1251–1286.

Reimer L. and Hawkes P. W. 1998. *Scanning electron microscopy: Physics of image formation and microanalysis*. Berlin: Springer. 529 p.

Reimold W. U. and Hörz F. 1986a. Experimental shock metamorphism of Witwatersrand quartzite. Proceedings of the Geocongress 86. pp. 53–57.

Reimold W. U. and Hörz F. 1986b. Textures of experimentally shocked (5.1–35.5 GPa) Witwatersrand quartzite. Proceedings, 17th Lunar and Planetary Science Conference. pp. 703–704.

Sigel G. H. and Marrone M. J. 1981. Photoluminescence in as-drawn and irradiated silica optical fibers: An assessment of the role of non-bridging oxygen defect centers. *Journal of Non-Crystalline Solids* 45:235–247.

Stähle V., Altherr R., Koch M., and Nasdala L. 2008. Shock-induced growth and metastability of stishovite and coesite in lithic clasts from suevite of the Ries impact crater (Germany). *Contributions to Mineralogy and Petrology* 155:457–472.

Stevens Kalceff M. A. 2009. Cathodoluminescence microcharacterization of point defects in α-quartz. *Mineralogical Magazine* 73:585–605.

Stevens Kalceff M. A. 2013. Cathodoluminescence microanalysis of silica and amorphized quartz. *Mineralogy and Petrology* 107:455–469.

Stevens Kalceff M. A. and Phillips M. R. 1995. Cathodoluminescence microcharacterization of the defect structure of quartz. *Physical Reviews B* 52:3122.

Stevens Kalceff M. A., Phillips M. R., Moon A. R., and Kalceff W. 2000. Cathodoluminescence microcharacterisation of silicon dioxide polymorphs. In *Cathodoluminescence in geosciences*, edited by Pagel M., Barbin V., Blanc P., and Ohnenstetter D. Berlin: Springer. pp. 193–224.

Stöffler D. and Langenhorst F. 1994. Shock metamorphism of quartz in nature and experiment: I. Basic observation and theory. *Meteoritics* 29:155–181.

Trepied L. and Doukhan J. C. 1978. Dissociated "a" dislocations in quartz. *Journal of Material Science* 13:492–498.

Trepmann C. A. and Spray J. G. 2005. Planar microstructures and Dauphiné twins in shocked quartz from the

Charlevoix impact structure, Canada. In *Large meteorite impacts III*, edited by Kenkmann T., Hörz F., and Deutsch A. Boulder, Colorado: Geological Society of America. pp. 315–328.

Trepmann C. A. and Spray J. G. 2006. Shock-induced crystal-plastic deformation and post-shock annealing of quartz: Microstructural evidence from crystalline target rocks of the Charlevoix impact structure, Canada. *European Journal of Mineralogy* 18:161–173.

Trepmann C. A., Gotte T., and Spray J. G. 2005. Impact-related Ca-metasomatism in crystalline target-rocks from the Charlevoix structure, Quebec, Canada. *Canadian Mineralogist* 43:553–567.

Trukhin A. N., Jansons J. L., Dyuzheva T. I., Lityagina L. M., and Bendeliani N. A. 2003. Luminescence of different modifications of crystalline silicon dioxide: Stishovite and coesite. *Solid State Communications* 127:415–418.

Trukhin A. N., Smits K., Chikvaidze G., Dyuzheva T. I., and Lityagina L. M. 2014. Luminescence of rutile structured crystalline silicon dioxide (stishovite). *Solid State Communications* 189:10–14.

Vernooij M. G. C. and Langenhorst F. 2005. Experimental reproduction of tectonic deformation lamellae in quartz and comparison to shock-induced planar deformation features. *Meteoritics & Planetary Science* 40:1353–1361.

Wirth R. 2004. Focused ion beam (FIB): A novel technology for advanced application of micro- and nanoanalysis in geosciences and applied mineralogy. *European Journal of Mineralogy* 16:863–876.

Wirth R. 2009. Focused ion beam (FIB) combined with SEM and TEM: Advanced analytical tools for studies of chemical composition, microstructure and crystal structure in geomaterials on a nanometre scale. *Chemical Geology* 261:217–229.